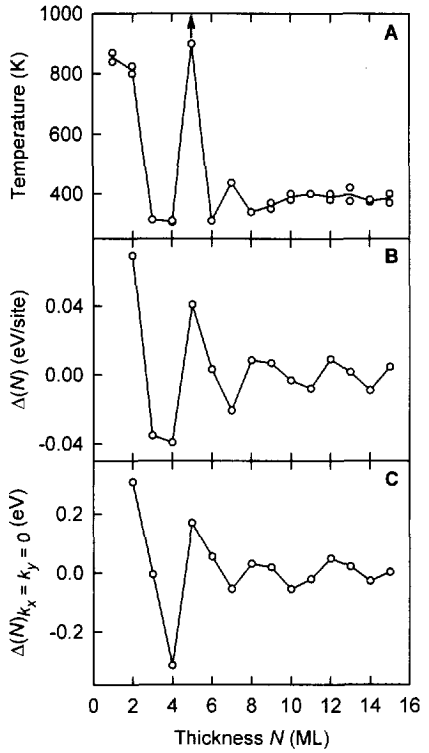

Fig. 3. (**A**) Temperatures at which films with an initial thickness of N begin to bifurcate. The $N = 5$ film is stable up to the highest temperature used in the experiment, and the arrow indicates that the data point represents a lower bound. (**B**) Calculated energy difference $\Delta(N) \equiv \frac{1}{2}[A(N+1) + A(N-1)] - A(N)$ against bifurcation as a function of N. (**C**) Results from the same calculation but without the summation over k_x and k_y.

well peak very close to the Fermi level at $E = 0$. Increasing the quantum-well width to $N = 5$ causes this state to drop below the Fermi level. This becomes the topmost-occupied quantum-well state for $N = 5$, and it is unusually deep below the Fermi level relative to the other cases (see Fig. 1). The whole subband has, on average, a lower energy, leading to an overall lower energy for the system. This argument suggests that film stability is mainly determined by the quantum-well state energies at the surface zone center. To verify this, Eq. 2 is reevaluated without summing over k_x and k_y. Indeed, the results (Fig. 3C) show the same general pattern for stability; namely, $N = 2$ and 5 are highly stable. Summing over a limited circle in k_x and k_y space leads to the same conclusion. A corollary is that detailed band structure features including the (111) neck do not play an important role.

The dominant issue for film stability is thus the phase-shift function Φ, which directly affects the quantum-well energies. In the present case, photoemission measurements provide an accurate determination of Φ, which is critical to the quantitative analysis presented above. Simple models based on one-dimensional potential wells, adopted in previous studies of metal films on semiconductors (*5*), generally do not lead to accurate quantum-well levels and are thus unable to explain our results quantitatively. Other effects that are important for metal-semiconductor interfaces, including an interface capacitor term (*5*), are found to be unimportant in the present case of a metal-metal interface. Using atomically uniform films in our experiment, questions regarding multiple steps do not arise, and the issue of stability reduces to a simple $N \rightarrow N \pm 1$ bifurcation as the first step toward roughening. For rough or nonuniform films, the situation can be far more complex, as there can be a multitude of paths for film-morphology evolution, including, for example, step bunching and pyramid formation.

A general strategy for stability engineering in nanostructures is thus to tailor the geometry to minimize the energies of the occupied states relative to the Fermi level. This is similar to the issue of stability for clusters (*13*) and nanowires (*14*), which prefer structures with a closed electronic shell. For Ag films considered here, adding one atomic layer generally leads to the addition of a partially occupied subband. The $N = 5$ case is an exception. Without a new subband below the Fermi level, it resembles a shell-closing point. Its topmost subband below the Fermi level is relatively deep, leading to a highly stable film. In going from clusters to wires and to films, the dimensionality of confinement is reduced from three to two and then to one. For films, the energy continuum in the other two dimensions tends to diminish this shell-closing effect. Nevertheless, quantum variations in stability remain an important effect, as shown in this study.

References and Notes

1. *Nanotechnology Research Directions*, Workshop Report by the Interagency Working Group on Nanoscience, Engineering and Technology, Committee on Technology, National Science and Technology Council for the Executive Office of the President of the United States of America, M. C. Roco, S. Williams, P. Alivisatos, Eds. (September 1999), available at www.sc.doe.gov/production/bes/iwgn.research.directions/welcome.htm.
2. J. J. Paggel, T. Miller, T.-C. Chiang, *Phys. Rev. Lett.* **81**, 5632 (1998).
3. A. R. Smith, K.-J. Chao, Q. Niu, C. K. Shih, *Science*, **273**, 226 (1996).
4. D. A. Evans, M. Alonso, R. Cimino, K. Horn, *Surf. Sci.* **376**, 1 (1997).
5. Z. Zhang, Q. Niu, C. K. Shih, *Phys. Rev. Lett.* **80**, 5381 (1998).
6. E. Tosatti, S. Prestipino, *Science* **289**, 561 (2000).
7. Y. Kondo, K. Takayanagi, *Science* **289**, 606 (2000).
8. J. J. Paggel, T. Miller, T.-C. Chiang *Science* **283**, 1709 (1999).
9. ———, *Phys. Rev. B* **61**, 1804 (2000).
10. T.-C. Chiang, *Surf. Sci. Rep.* **39**, 181 (2000).
11. N. V. Smith, L. F. Mattheiss, *Phys. Rev. B* **9**, 1341 (1974).
12. V. K. Kumikov, Kh. B. Khokonov, *J. Appl. Phys.* **54**, 1346 (1983).
13. W. D. Knight *et al.*, *Phys. Rev. Lett.* **52**, 2141 (1984).
14. A. I. Yanson, I. K. Yanson, J. M. van Ruitenbeek, *Nature* **400**, 144 (1999).

15. Supported by the U.S. National Science Foundation (grants DMR-99-75470 and DMR-99-75182 to T.C.C) and the U.S. Department of Energy (grant DEFG02-97ER45632 to M.Y.C.). We acknowledge the Petroleum Research Fund, administered by the American Chemical Society, and the U.S. Department of Energy, Division of Materials Sciences (grant DEFG02-96ER45439), for partial support of the synchrotron beamline operation and the central facilities of the Materials Research Laboratory. The Synchrotron Radiation Center of the University of Wisconsin–Madison, where the experiment was done, is supported by the U.S. National Science Foundation (grant DMR-00-84402).

24 January 2001; accepted 19 March 2001

Proposed Square Spiral Microfabrication Architecture for Large Three-Dimensional Photonic Band Gap Crystals

Ovidiu Toader and Sajeev John

We present a blueprint for a three-dimensional photonic band gap (PBG) material that is amenable to large-scale microfabrication on the optical scale using glancing angle deposition methods. The proposed chiral crystal consists of square spiral posts on a tetragonal lattice. In the case of silicon posts in air (direct structure), the full PBG can be as large as 15% of the gap center frequency, whereas for air posts in a silicon background (inverted structure) the maximum PBG is 24% of the center frequency. This PBG occurs between the fourth and fifth bands of the photon dispersion relation and is very robust to variations (disorder) in the geometrical parameters of the crystal.

Photonic band gap (*1, 2*) materials are artificial dielectric crystals with a periodicity on the optical wavelength scale. Because of a confluence of macroscopic (Bragg) and microscopic scattering resonances, these crystals can create a bound-state spectrum for electromagnetic waves with wavelengths comparable to the lattice constant. It is this

ability to "cage" or localize (*3*) light that makes the photonic crystal suitable for a variety of passive and active microphotonic devices as well as optical microcircuitry (*4*).

Large-scale microfabrication of three-dimensional (3D) photonic crystals with band gaps centered at a wavelength shorter than 2 μm has been a major materials science challenge over the past decade. Although theory (*5*) has predicted that an inverse diamond lattice of overlapping air spheres in a high refractive index background will provide a large, full 3D PBG, the synthesis of structures of this type (*6*) has proved difficult. Attention has shifted to other diamond-like structures such as the woodpile structure (*7, 8*), which has a full PBG opening between the second and third photonic bands. Even in this case, complex and time-consuming microlithography is required. Alternatively, self-assembly methods have provided large-scale face-centered cubic (fcc) inverse opal PBG materials (*9*) with a gap of roughly 5% of the center frequency opening between the eighth and ninth bands. However, the PBG in this case is relatively unstable to disorder effects. These and other studies (*10, 11*) have created the impression that a large and robust 3D PBG can only be obtained in the (fundamental) gap between the second and third bands in any photonic crystal.

Here, we propose an alternative photonic crystal architecture consisting of square spiral posts in a tetragonal lattice. This structure has a large and robust 3D PBG occurring between the fourth and fifth electromagnetic bands and is amenable to large-scale microfabrication using glancing angle deposition (GLAD) techniques (*12, 13*). Figure 1 depicts such a crystal and describes the geometry of its building blocks. The tetragonal crystal has lattice constants **c** along the *z* axis and **a** along the *x* and *y* axes. We choose our unit of length to be **a**. The building block of the crystal is made from a coil of pitch **c** (Fig. 1, side view inset) with a single loop whose transverse cross section is a square with edges of length **L** (Fig. 1, top view inset). The pitch is the same as the lattice constant in the *z* direction, and the coil is wrapped around the *z* axis. Each of the segments of the coil is coated with a cylinder of radius **r** (Fig. 1, top view inset) whose dielectric constant is ε_s. The spirals are embedded in a material whose dielectric constant is ε_b. We impose no restriction on the size of **L** relative to **a** or on overlapping between adjacent spirals.

Spiral post lattices with microscale features have previously been synthesized using the GLAD method. In this technique, complex 3D structures can be fabricated by combining oblique vapor deposition and precisely controlled motion of a two-dimensionally patterned substrate (*12, 13*). Posts consisting of semiconductors, metals, metal oxides, and fluorides can be grown using GLAD. However, no blueprint defining the geometrical parameters for GLAD-based PBG synthesis has been proposed. Previous designs involving circular posts (*14*) involve a phase shift between adjacent spirals and are not suited to microfabrication. Our square spiral posts can serve as templates for growing PBG materials from an even larger range of materials. In this case, a high refractive index material may be infiltrated to fill the void regions between the posts, with the posts subsequently removed by some selective etching process, leaving behind an "inverted structure." Two-photon lithography can also be used to create a tem-

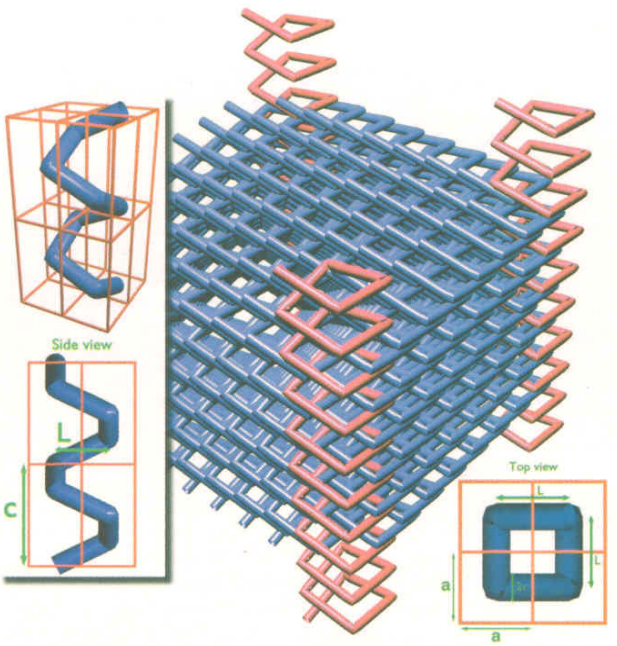

Fig. 1. Tetragonal square spiral photonic crystal. The crystal shown here has a solid filling fraction of 30%. For clarity, spirals at the corners of the crystal are highlighted with a different color and height. The tetragonal lattice is characterized by lattice constants **a** and **c**. The geometry of the square spiral is illustrated in the insets and is characterized by its width, **L**, cylinder radius, **r**, and pitch, **c**. The top left inset shows a single spiral coiling around four unit cells.

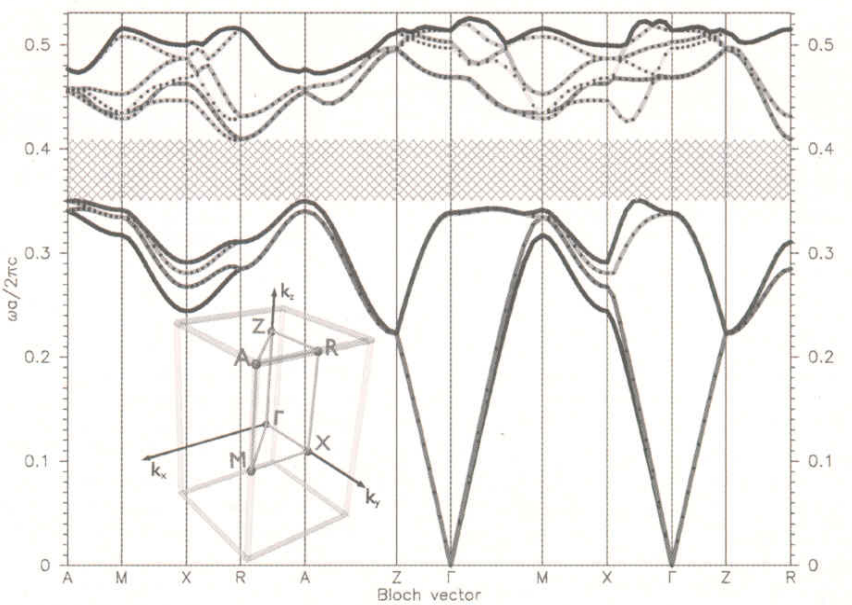

Fig. 2. Band structure for the direct structure crystal characterized by [**L**,**c**,**r**] = [1.6,1.2,0.14] and f_{spiral} = 30%. The lengths are given in units of **a**, the lattice constant. The width of the PBG is 15.2% relative to the center frequency for ε_b = 1 and ε_s = 11.9. The positions of high symmetry points are illustrated in the inset.

Department of Physics, University of Toronto, 60 St. George Street, Toronto M5S-1A7, Canada. E-mail: ovi@physics.utoronto.ca (O.T.); john@physics.utoronto.ca (S.J.)

plate for such a photonic crystal. In this approach, a two-photon microscope focuses light in a suitably prepared liquid, causing polymerization (solidification) wherever the microscope focuses (*15*).

For the purpose of illustration, we choose the dielectric constant of the material with high index to be that of Si, which is approximately 11.9 at wavelengths larger than 2 μm (*16*). The direct structure crystal is defined by $\varepsilon_b = 1$ and $\varepsilon_s = 11.9$, and the inverted structure crystal is defined by $\varepsilon_b = 11.9$ and $\varepsilon_s = 1$. Body- and face-centered tetragonal lattices can be visualized by imposing a $\underline{\mathbf{c}}/2$ translation along the z axis between adjacent spirals in the crystal. Chutinan and Noda (*14*) have studied photonic crystals built from circular spiral elements on simple cubic, fcc, and body-centered cubic (bcc) lattices. It is reported that in the case of a crystal with $\varepsilon_b = 1$ and $\varepsilon_s = 12.25$ the maximum band gap is only 3%, and it appears when the simple cubic lattice is deformed into a tetragonal lattice. For the case of bcc and fcc lattices, full photonic gaps of around 17% open between the second and third bands. Because the phase shift between adjacent spirals cannot easily be attained using the present GLAD technique, we focus our attention on the simple tetragonal crystal lattice.

In our calculations, we used the plane waves expansion method (*5*) with more than 1400 plane waves. The Fourier coefficients of the dielectric have been calculated by fast Fourier transform with a sampling of 512^3 points in one unit cell. In the case of the direct structure crystal, we find a local maximum of the relative band gap as a function of $\underline{\mathbf{L}}$, $\underline{\mathbf{c}}$ and $\underline{\mathbf{r}}$ for the case $[\underline{\mathbf{L}},\underline{\mathbf{c}},\underline{\mathbf{r}}] = [1.6,1.2,0.14]$. We find a sizable gap for a wide range of filling factors of the spiral component, f_{spiral}. At small f_{spiral}, the individual spirals are disconnected and the air forms the connected component in the system, whereas for large f_{spiral}, both the air and spirals form connected components. We show the photonic band structure and the positions of the high symmetry points in the Brillouin zone for the direct structure crystal with the optimized parameters (Fig. 2). A large PBG of 15.2% relative width opens between the fourth and fifth bands. The upper edge of the photonic band gap closes at R point, and only two bands (the fifth and sixth) contribute to the spectrum around the upper edge. These lead to an even larger pseudogap of roughly 25% of the center frequency.

For the corresponding inverted structure crystal (characterized by $\varepsilon_b = 11.9$ and $\varepsilon_s = 1$), we find a local maximum of the relative band gap as a function of $\underline{\mathbf{L}}$, $\underline{\mathbf{c}}$, and $\underline{\mathbf{r}}$ located at $[\underline{\mathbf{L}},\underline{\mathbf{c}},\underline{\mathbf{r}}] = [1.5,1.7,0.33]$. The total density of states (DOS) for this structure is shown in the inset of Fig. 3. The optimized inverse square spiral structure described above can be made using a three-stage process. In the first stage, a silica-based square spiral template (with nonoverlapping posts) is created using GLAD. The template (required to create a 23.6% PBG) involves a silica volume-filling fraction of 79% and a significant overlap of the spiral arms (Fig. 3). This overlapping structure may be achieved in stage two by immersing the template from stage one into a liquid solution. Further silica growth can be achieved using a sol-gel process (*9*, *17*). Once the template reaches the silica volume-filling fraction shown in Fig. 3, it can be infiltrated (stage three) with silicon using chemical vapor deposition, and the original silica template is removed using a hydrofluoric acid etch (*9*).

We also studied the size of the full photonic band gap as a function of the index contrast defined as n_s/n_b for the direct structure and n_b/n_s for the inverse structure, where $n_b = \varepsilon_b^{1/2}$ and $n_s = \varepsilon_s^{1/2}$. The threshold index contrast for creating a complete 3D PBG is 2.25 for the direct structure and 2.2 for the inverse structure.

The square spiral photonic crystals in a simple tetragonal lattice offer a new avenue to large-scale microfabrication of photonic crystals with a very large and complete 3D PBG. Unlike the optimized inverse diamond structure and its variants, which have been the driving force behind many complex microfabrication strategies, the present blueprint can be realized using a straightforward glancing angle deposition method. Our PBG material blueprint belongs to a relatively unique class of photonic crystals with a large gap between the fourth and fifth photon dispersion bands and is highly robust to disorder effects (*18*). The optimized crystal has a large full PBG, and the direct structure has a considerably larger pseudogap. This gap is very stable with respect to the crystal's geometrical parameters and also relatively insensitive to the transition from a topologically disconnected to a connected high dielectric component.

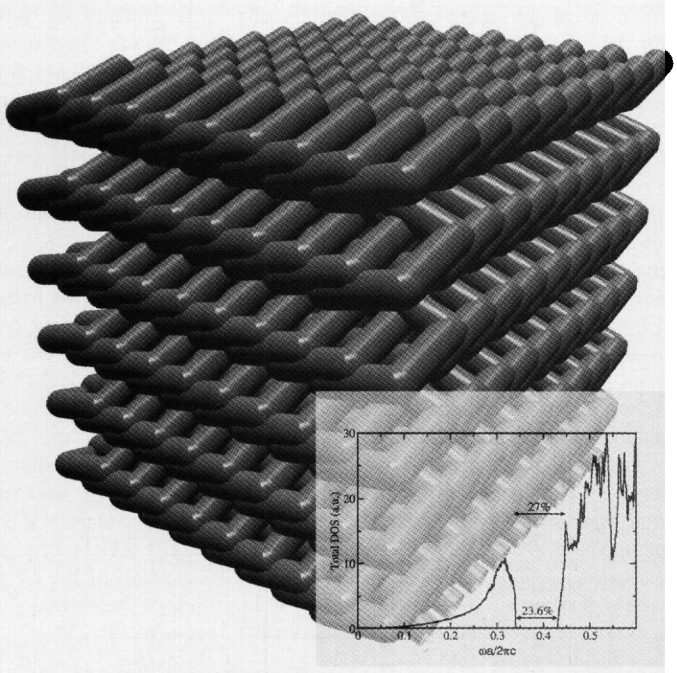

Fig. 3. Template for the optimized inverted structure characterized by $[\underline{\mathbf{L}},\underline{\mathbf{c}},\underline{\mathbf{r}}] = [1.5,1.7,0.33]$. The solid filling fraction is 79%. The Si crystal obtained by inverting this template has a 23.6% PBG and a 27% pseudogap. The corresponding total DOS is shown in the inset (arbitrary units).

References and Notes

1. S. John, *Phys. Rev. Lett.* **58**, 2486 (1987).
2. E. Yablonovitch, *Phys. Rev. Lett.* **58**, 2059 (1987).
3. S. John, *Phys. Rev. Lett.* **53**, 2169 (1984).
4. J. D. Joannopoulos, P. R. Villeneuve, S. Fan, *Nature* **386**, 143 (1997).
5. K. M. Ho, C. T. Chan, C. M. Soukoulis, *Phys. Rev. Lett.* **65**, 3152 (1990).
6. E. Yablonovitch, T. J. Gmitter, K. M. Leung, *Phys. Rev. Lett.* **67**, 2295 (1991).
7. K. M. Ho, C. T. Chan, C. M. Soukoulis, R. Biswas, M. Sigalas, *Solid State Commun.* **89**, 413 (1994).
8. H. S. Sözüer, J. P. Dowling, *J. Mod. Opt.* **41**, 231 (1994).
9. A. Blanco *et al.*, *Nature* **405**, 437 (2000).
10. H. S. Sözüer, J. W. Haus, *J. Opt. Soc. Am. B* **10**, 296 (1993).
11. Y.-C. Tsai, J. B. Pendry, K. W.-K. Shung, *Phys. Rev. B* **59**, 10401 (1999).
12. K. Robbie, M. J. Brett, *J. Vac. Sci. Technol. B* **15**, 1460 (1997).
13. K. Robbie, J. C. Sit, M. J. Brett, *J. Vac. Sci. Technol. B* **16**, 1115 (1998).
14. A. Chutinan, S. Noda, *Phys. Rev. B* **57**, 2006 (1998).
15. B. H. Cumpston *et al.*, *Nature* **398**, 51 (1999).
16. E. D. Palik, Ed., *Handbook of Optical Constants of Solids* (Academic Press, Orlando, FL, 1985).
17. W. Stöber, A. Fink, E. Bohn, *J. Colloid Interface Sci.* **26**, 62 (1968).
18. O. Toader, S. John, in preparation.

19. This work was supported in part by the National Sciences and Engineering Research Council of Canada and the John Simon Guggenheim Foundation.

1 February 2001; accepted 28 March 2001